

Stereo-digital image correlation in the behavior investigation of CFRP-steel composite members

Yun-Tong Dai^{1,2}, Hai-Tao Wang³, Tian-Yuan Ge^{1,2}, Gang Wu³,
Jian-Xiao Wan⁴, Shuang-Yin Cao⁴, Fu-Jun Yang^{1,2} and Xiao-Yuan He^{*1,2}

¹ Jiangsu Key Laboratory of Engineering Mechanics, Southeast University, Nanjing, P.R. China

² Department of Engineering Mechanics, Southeast University, Nanjing, P.R. China

³ Key Laboratory of Concrete and Prestressed Concrete Structures of the Ministry of Education, Southeast University, Nanjing, P.R. China

⁴ School of Civil Engineering, Southeast University, Nanjing, P.R. China

(Received April 21, 2016, Revised January 16, 2017, Accepted February 25, 2017)

Abstract. The application of carbon fiber reinforced polymer (CFRP) in steel structures primarily includes two categories, i.e., the bond-critical application and the contact-critical application. Debonding failure and buckling failure are the main failure modes for these two applications. Conventional electrometric techniques may not provide precise results because of the limitations associated with single-point contact measurements. A nondestructive full-field measurement technique is a valuable alternative to conventional methods. In this study, the digital image correlation (DIC) technique was adopted to investigate the bond behavior and buckling behavior of CFRP-steel composite members. The CFRP-to-steel bonded joint and the CFRP-strengthened square hollow section (SHS) steel column were tested to verify the suitability of the DIC technique. The stereo-DIC technique was utilized to measure continuous deformation. The bond-slip relationship of the CFRP-to-steel interface was derived using the DIC data. Additionally, a multi-camera DIC system consisting of four stereo-DIC subsystems was proposed and applied to the compressive test of CFRP-strengthened SHS steel column. The precise buckling location and CFRP delamination of the CFRP-strengthened SHS steel column were identified. The experimental results confirm that the stereo-DIC technique can provide effective measurements for investigating the behaviors of CFRP-steel composite members.

Keywords: CFRP; steel; bond behavior; buckling behavior; digital image correlation

1. Introduction

Fiber reinforced polymer (FRP) composites have a significant role in the strengthening of structures due to advantages such as a high strength-to-weight ratio and superior corrosion resistance (Bakis *et al.* 2002). Numerous studies of FRP-strengthened concrete structures have been conducted in the past two decades (Ali-Ahmad *et al.* 2006, Abdelrahman and El-Hacha 2011, Shi *et al.* 2012, Daud *et al.* 2015, Hadji *et al.* 2016). In recent years, the FRP-strengthened steel structure has become a research focus (Shaht and Fam 2006, 2009, Zhao and Zhang 2007, Bocciarelli *et al.* 2009, Teng *et al.* 2012, Park and Yoo 2015). Based on existing findings (Teng *et al.* 2012), the use of FRP in steel structures can be divided into two categories, namely, the bond-critical application and the contact-critical application. The bond-critical application depicts that the interfacial shear stress transfer in the adhesive layer that bonds the FRP and the steel is a decisive factor in ensuring effective strengthening, whereas the interfacial normal stress transfer in the ongoing contact between the FRP and the steel is the determining factor in the case of contact-critical application. In CFRP-streng-

thened steel members, the externally-bonded CFRP strengthening for improving the flexural and fatigue behaviors belongs to the first category, whereas the CFRP-confined steel columns can be assigned to the second category.

For the externally-bonded CFRP strengthened steel members, many studies have demonstrated that debonding failure is a main failure mode (Zhao and Zhang 2007, Bocciarelli *et al.* 2009, Teng *et al.* 2012). Therefore, understanding the bond behavior between CFRP and steel is critical. The bond joints are usually employed to study the bond behaviors of CFRP-to-steel interfaces. As previously reported (Fawzia *et al.* 2010, Yu *et al.* 2012, Wu *et al.* 2012), the deformation measurements of the joints were substantially dependent on conventional electrometric techniques, such as electrical resistance strain gauge, displacement transducer, and extensometer. However, single-point contact measurements are involved, and the surface preparation and the instrument arrangement are tedious and time-consuming. The bond-slip relationship, which depicts the relationship between the relative slip and the interfacial shear stress, is crucial for characterizing the bond behaviors of CFRP-to-steel interfaces, which were previously derived from the CFRP strains that were measured with strain gauges attached to the CFRP surfaces. The relative slip and interfacial shear stress were commonly obtained by the integral operation and differential operation

*Corresponding author, Professor,
E-mail: mmhxy@seu.edu.cn

of strain data, respectively. Because the measured displacement and strain data are limited and discrete, the results comprised the average value among the limited measuring points. Thus, this conventional strain gauge method may produce unavoidable error in the bond-slip relationship of CFRP-to-steel interfaces.

CFRP sheets were frequently employed as external reinforcement for columns, especially square hollow section (SHS) steel columns. Local buckling may occur in short SHS steel columns when subjected to axial compression. CFRP has been employed in SHS steel columns against local buckling. In previous studies (Shaaf and Fam 2006, 2009), the displacement transducers and strain gauges were placed on the anticipated buckling area to evaluate the buckling behavior. This method is unable to obtain the exact buckling location, which causes inaccurate measurement results.

The preceding analysis concluded that some limitations exist in the conventional electrometric techniques that are applied to evaluate the bond and buckling behaviors of CFRP-steel composite members. A full-field measurement technique is an effective solution to this problem. The digital image correlation (DIC) technique is a noncontact, full-field technique that measures surface shape, displacement and strain (Sutton *et al.* 2009). Since its inception in the early 1980s (Peters and Ranson 1982), the DIC technique underwent many modifications that have improved its computation efficiency and accuracy (Pan *et al.* 2013, Shao *et al.* 2015). Currently, the stereo-DIC technique has provided a complete and mature testing system in various scientific and engineering fields (Pan *et al.* 2012, Fagerholt *et al.* 2013, Malesa *et al.* 2013, Busca *et al.* 2014) due to its simple setup and preparation, easy and automatic processing, and full-field and noncontact measurement. Additionally, the DIC technique has been applied to some studies of composites (Ghiassi *et al.* 2013, Kumar *et al.* 2013, Zhu *et al.* 2014). Therefore, the suitability of the DIC technique in measuring the mechanical behaviors of CFRP-steel composite members should be investigated.

This paper reports the effectiveness of the DIC technique in investigating the bond and buckling behaviors of CFRP-steel composite members. A study of the bond behavior was conducted using the CFRP-to-steel bonded joints, whereas a study of the buckling behavior was implemented using the CFRP-strengthened SHS steel columns. The stereo-DIC technique was utilized to measure the continuous displacement and strain data of the CFRP plate and the steel to obtain the bond-slip relationship. A multi-camera DIC system that consists of four stereo-DIC subsystems was proposed and applied to the compressive tests of CFRP-strengthened SHS steel columns. The multi-camera DIC system can indicate the exact position and shape of local buckling on the full surface of a column.

2. Stereo-DIC technique

The stereo-DIC technique is a nondestructive full-field measurement technique that combines digital image correlation with binocular stereo-vision. It captures images

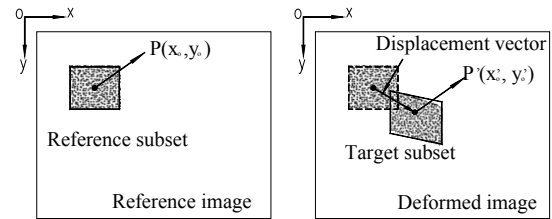


Fig. 1 Schematic of DIC

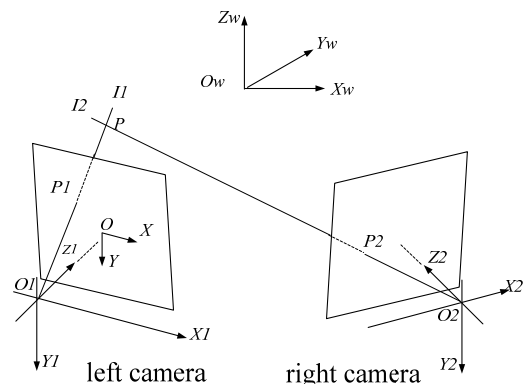


Fig. 2 Schematic of binocular stereo-vision

of the testing object before and after deformation, tracks the speckle patterns on the object surface via correlation calculation, and realizes the noncontact, full-field, and three-dimensional measurement of shape, displacement and strain (Sutton *et al.* 2009).

The basic principle of DIC is matching the same physical point between a reference image and a deformed image. As illustrated in Fig. 1, a square subset of $(2M + 1) \times (2M + 1)$ pixels in the reference image is selected and employed to search for its corresponding target subset in the deformed image with the correlation function. The center points of the reference and target subsets define the displacement vector, thus, the displacement distribution can be obtained. The strain distribution can be calculated from the displacement distribution.

Based on binocular stereo-vision, three-dimensional reconstruction is realized. Two cameras are used to capture two-dimensional images of the testing object from different perspectives; the disparity of the corresponding image points in different images is calculated and analyzed; and three-dimensional information of the object is obtained. As shown in Fig. 2, $P(X, Y, Z)^T$ is a three-dimensional point to be measured and $P_1(u_1, v_1)^T$ and $P_2(u_2, v_2)^T$ are its projections in images of the two cameras. By combining the image coordinates of points P_1 and P_2 with the intrinsic parameters and extrinsic parameters of the two cameras, a three-dimensional coordinate of the physical point P in the World Coordinate System can be obtained using triangulation theory. Details about the principle have been provided in the previous study (Sutton *et al.* 2009).

3. Experimental program

3.1 Shear test of CFRP plate-to-steel bonded joints

The bond-slip relationship is an important aspect of the bond behavior of CFRP-to-steel interfaces. This relationship can be experimentally obtained from the shear test of CFRP-to-steel bonded joints. The single-shear test method was recommended to measure the bond-slip relationship of CFRP plate-to-steel interfaces (Zhao and Zhang 2007, Teng *et al.* 2012). The bond-slip relationship was generally derived from the CFRP strain measured with strain gauges in previous studies (Fawzia *et al.* 2010, Yu *et al.* 2012, Wu *et al.* 2012). The conventional method is not sufficiently precise because the results comprise the average value among the limited measuring points. The DIC technique can directly provide the continuous deformation distribution for the bond-slip relationship. With sufficient density, the obtained data will effectively improve the accuracy of the results.

In this paper, the single-shear test was combined with the stereo-DIC technique to investigate the bond behavior of the CFRP-to-steel interface. To compare the measurement results between the conventional electrometric technique and the DIC technique, specimens with equivalent parameters were divided into two groups, namely, the strain gauge group and the DIC group. An issue to note is that only one group of specimens (CFRP plate: length of 350 mm, width of 50 mm, thickness of 1.4 mm;

adhesive: Sika_30, thickness of 0.5 mm) is employed as an example to demonstrate the effectiveness of the DIC technique in investigating the bond behavior. Additional results about the bond behavior of the CFRP-to-steel interface are presented and discussed elsewhere (Wang *et al.* 2016).

The experimental setup is illustrated in Fig. 3. The setup primarily included two complementary metal oxide semiconductor (CMOS) cameras (IDS UI-3370CP, 2048×2048 pixels), two Kowa lens (focal length of 25 mm), two light-emitting diode (LED) light sources, a testing machine and a computer. The specimens were subjected to tensile loads with a displacement rate of 0.003 mm/s until failure on a servo-hydraulic testing system with a loading capacity of 1000 kN. The continuous loading process was recorded once per second via the stereo-DIC system with the cameras' angle of 23.49° and area of interest (AOI) of $140 \times 380 \text{ mm}^2$.

3.2 Compressive test of SHS steel column strengthened with CFRP sheets

CFRP sheets have been frequently employed in the strengthening of the SHS steel columns against buckling. The effect of CFRP sheets on the buckling behavior was previously evaluated with displacement transducers and strain gauges that were placed on the area where buckling was anticipated (Shaath and Fam 2006, 2009). The uncertainty in the occurrence position of buckling may produce errors in the measurement results. However, the DIC technique can directly capture the buckling shape by obtaining the continuous deformation of the exact buckling area. The typical failure mode can also be presented with the full-field deformation distribution.

Because the four sides of a square column cannot be covered by a single stereo-DIC system, the stereo-DIC technique is expanded with a synchronous acquisition system of multiple cameras to form the multi-camera DIC system. The proposed multi-camera DIC system in this study consists of four stereo-DIC subsystems, which are distributed to cover the four sides of the testing column. Fig. 4 schematically shows the multi-camera DIC system. Each subsystem, which is composed of two cameras, measures the four sides of the column. Deformation of each side on the column surface can be obtained from the corresponding subsystem. The eight cameras synchronously capture images under the control of a synchronous signal trigger. Cameras are assembled in a series connection in each subsystem; each subsystem is subsequently connected to each acquisition card of the computer. The system stability has been investigated by the authors' group (Liu *et al.* 2013). Compared with the stereo-DIC system, the multi-camera DIC system is more suitable for column measurement.

In this paper, the buckling behavior of the CFRP-strengthened SHS steel column was examined with the proposed multi-camera DIC system. Note that only one group of specimens is employed as an example to demonstrate the effectiveness of the DIC technique in investigating the buckling behavior of the CFRP streng-

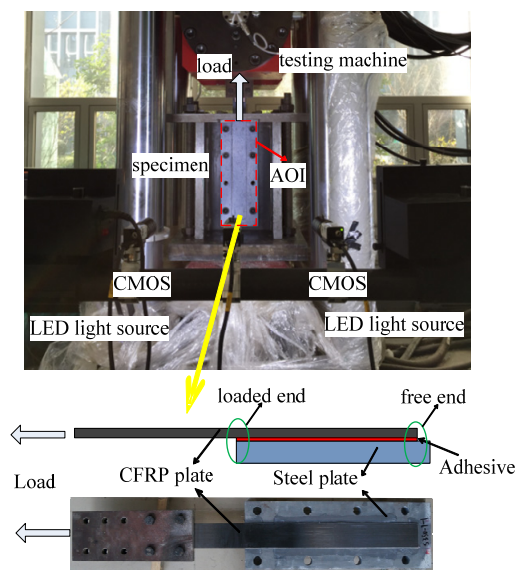


Fig. 3 Experiment setup and the bonded joint

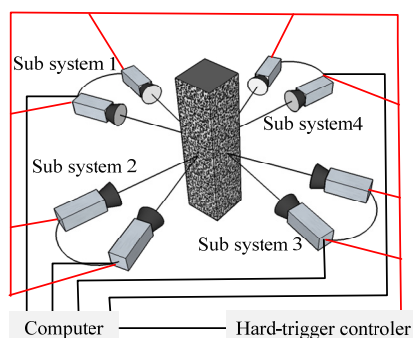


Fig. 4 Multi-camera DIC system for column measurement

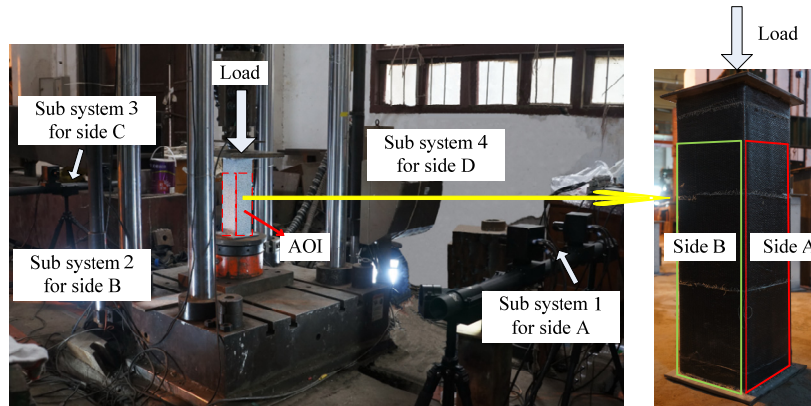


Fig. 5 Experiment setup of multi-camera DIC system and the specimen

thened SHS steel column. The section size and length of the example columns were 150 mm × 150 mm × 2.5 mm and 500 mm, respectively. The SHS steel column, which was wrapped with both longitudinally and transversely oriented CFRP sheets, was compared with the control column. Additional discussions about the mechanical behavior of the SHS steel columns strengthened with CFRP sheets will be presented elsewhere.

The test setup is shown in Fig. 5. The upper and lower ends of the columns were connected by a hinge support to mechanical testing system, and columns were loaded in compression until failure. Load control was utilized in the preliminary load stage, whereas displacement control was implemented in a subsequent stage. Because the exact occurrence of out-of-plane deformation and buckling are uncertain, exact deformation data are difficult to obtain by attaching displacement transducers and strain gauges. Thus, the four sides of the column were monitored by a multi-camera DIC system consisting of four stereo-DIC subsystems. The system primarily included eight charge coupled device (CCD) cameras (Point Grey GRAS-50S5M-C, 2448 × 2048 pixels), eight Kowa lens (focal length of 25 mm) and four LED light sources. Each subsystem kept an AOI of 150 × 400 mm², a cameras' angle of about 21.04° and a frame rate of 1 f/s.

Table 1 DIC parameters selection

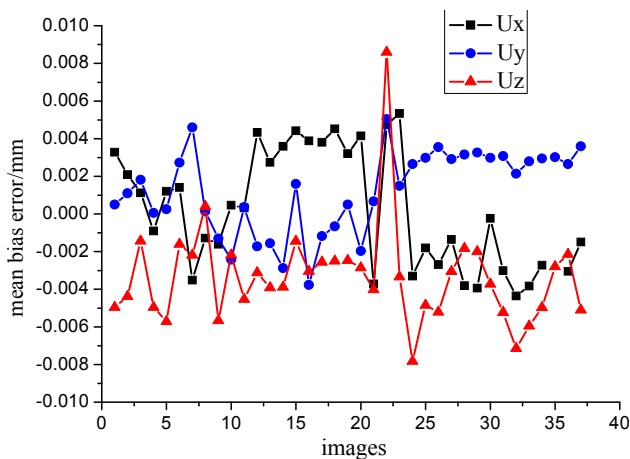
Parameters	Shear test	Compressive test
Subset size (pixels)	29 × 29	31 × 31
Subset step (pixels)	7	17
Size of strain calculation window (points)	15 × 15	15 × 15

3.3 Stereo-DIC measurements in the tests

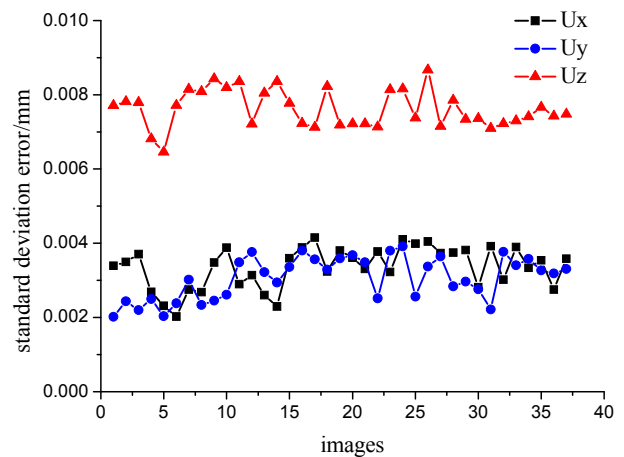
The DIC measurement is closely related to the quality of the speckle pattern. The speckle pattern was created via spray paint in the tests. A thin coating of white paint was first sprayed onto the specimen surface and then a spot distribution of black paint was sprayed on top to form the random speckle pattern for DIC measurements.

To realize the three-dimensional reconstruction in stereo-DIC, the intrinsic and extrinsic parameters of the two cameras should be determined through the system calibration. The size of calibration panel is usually chosen according to the AOI. The calibration panels in size of 275 × 200 mm² and 315 × 315 mm² were respectively used for the two tests.

The calculating parameters including the subset size,



(a) Mean bias error



(b) Standard deviation error

Fig. 6 Noise analysis

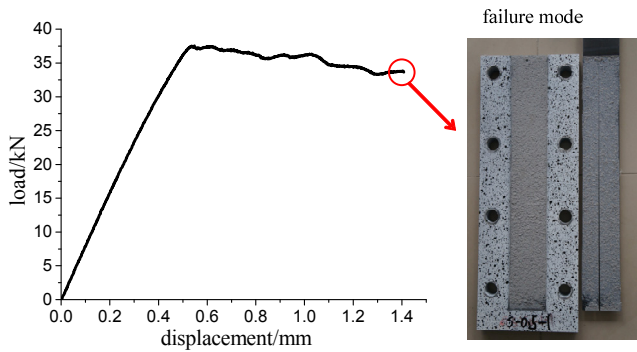


Fig. 7 Load-displacement curve and specimen failure

subset step and size of strain calculation window, have vital influences on DIC results. In subset-based DIC, the increasing subset size can smooth the displacements, but also decrease the spatial resolution. Each subset must contain enough speckles with good contrast features. In this paper, in order to achieve an appropriate balance between accuracy and spatial resolution, one subset was set to contain three to five speckles. The subset step is the distance between the grid points in pixel. As each grid point represents one single data point of the DIC result, the step limits the spatial resolution. Additionally, to obtain reasonable and accurate strain estimation, the size of local strain calculation window is also crucial. A small strain calculation window cannot suppress the noise of the displacements, whereas a large one may lead to smoother but unreasonable results. The parameters selected for the two tests are presented in Table 1.

During the recording, various noises, for instance, ambient noises, illumination fluctuation and thermal noises, are unavoidably introduced into the digital images. For the purpose of estimating the measuring system accuracy, motionless tests were performed on the testing specimens. Take the shear test of CFRP plate-to-steel bonded joints as an example, cameras recorded several images of the testing specimen without applying any load. The noise of the computed displacements via stereo-DIC (Ke *et al.* 2011, Wang *et al.* 2011) can be analyzed with two errors: mean bias error (i.e., the systematic error) and standard deviation

error (i.e., the random error), as shown in Fig. 6. For the in-plane displacements U_X and U_Y , the mean bias error fluctuated between -0.004 mm and 0.004 mm, and the standard deviation error was measured to be 0.003 mm. While a value range from -0.008 mm to 0.008 mm of the mean bias error and a standard deviation error of 0.0075 mm were determined for the out-of-plane displacement U_Z .

4. Results and discussion

4.1 Bond behavior investigation of CFRP-to-steel interface

The load-displacement curve and the failure mode are presented in Fig. 7. The debonding occurred within the adhesive layer, which indicates a cohesive failure mode. The cohesive failure mode was encouraged considering that the strength of adhesive was fully utilized.

Instead of deriving the relative slip from the integral operation of limited strain gauge data that has been reported in previous studies (Fawzia *et al.* 2010, Yu *et al.* 2012, Wu *et al.* 2012), the continuous displacements of the CFRP plate and steel in this study were directly obtained with DIC software PMLAB DIC-3D_2014a. Fig. 8 presents the typical displacement distribution on the CFRP and steel surfaces in the length and width directions. The CFRP displacement was taken to be the average value across the 10 mm-wide central origin of CFRP plate, whereas the steel displacement was derived as the average of two regions in width of 5 mm on both sides. It is evident that CFRP displacement gradually decreased with an increase in the distance from the loaded end, whereas the steel displacement remained constant along the length direction. The steel displacement was supposed to be almost the rigid body displacement induced by the deformation of the test rig. Due to the difficulty of measuring the displacement of the steel surface beneath the CFRP plate and the assumption that the displacement of the steel surface remains constant along the width direction, the displacement difference between the CFRP and steel on both sides can be considered to be the relative slip of the CFRP-to-steel interface. As shown in Fig. 8, the relative slip gradually decreased with the increasing distance from the loaded end

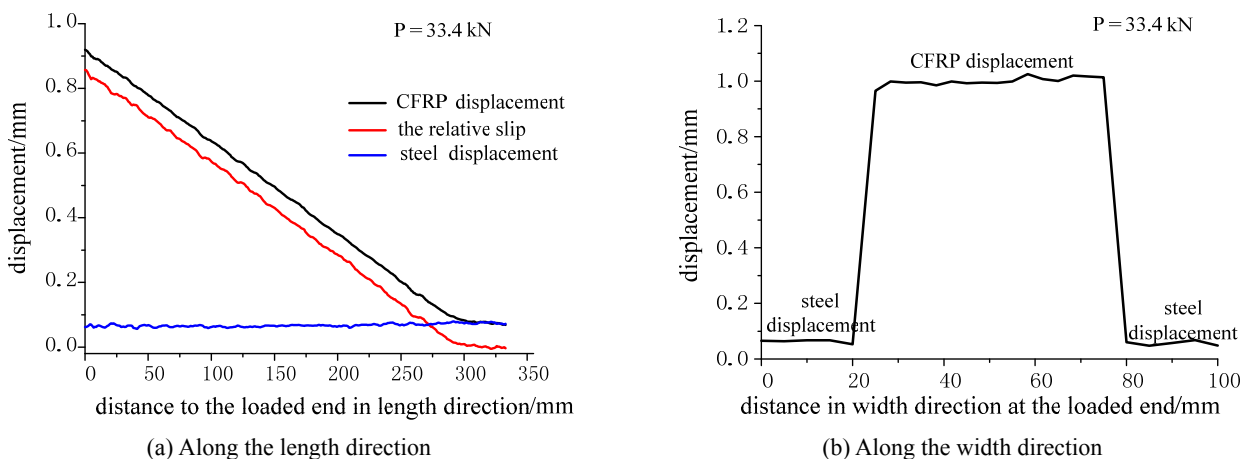


Fig. 8 Displacement and relative slip distribution of the specimen

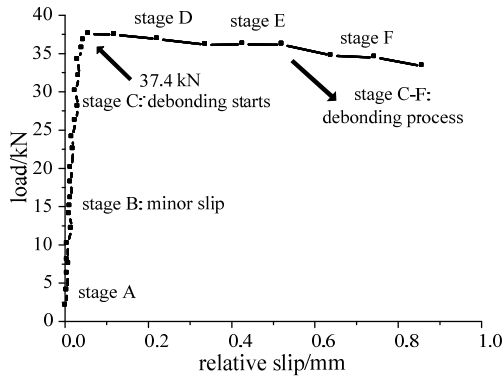


Fig. 9 Load-slip curve of the loaded end

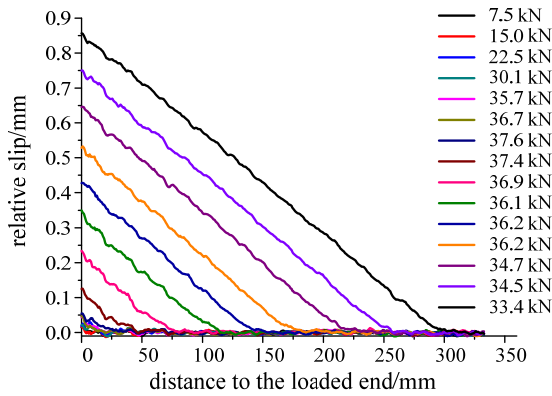


Fig. 10 Relative slip distribution on CFRP-to-steel interface

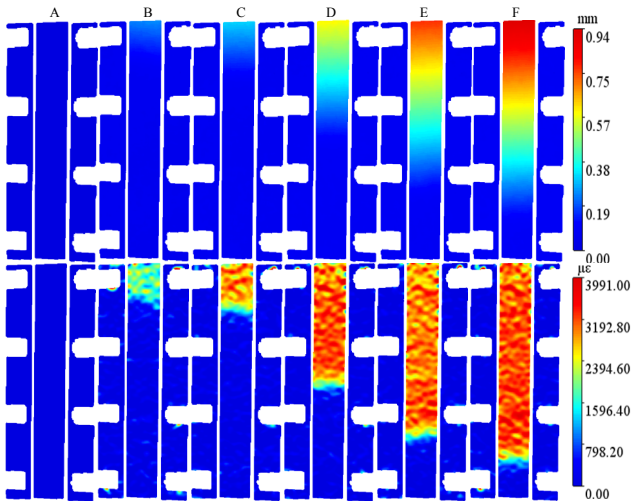


Fig. 11 Deformation fields on the specimen surface at different stages

to the free end.

Fig. 9 plots the typical load-slip relationship of the loaded end. In the initial load stages, a minor slip that linearly increased with the load was observed. As the applied load increased to 37.4 kN, the debonding occurred at the loaded end. Subsequently, the load-slip curve remained in a plateau until final failure. The plateau from stage C to stage F recorded the gradual shear debonding process of the bonded interface.

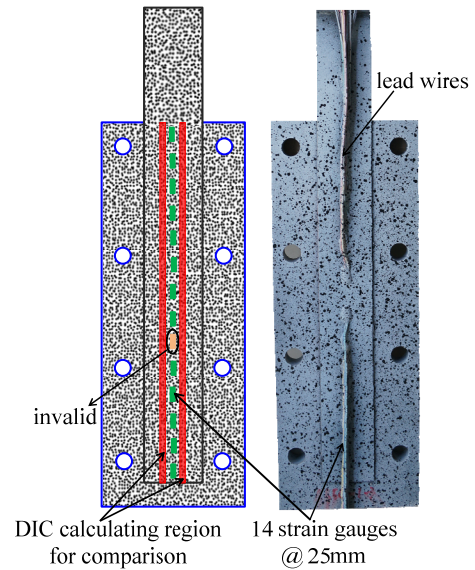


Fig. 12 Strain gauge group

Fig. 10 presents the relative slip distribution on the CFRP-to-steel interface that was obtained via stereo-DIC. In the preliminary stages of loading, only the loaded end experienced a slight slip. With an increase in applied load, the relative slip gradually increased and extended in the length direction. Debonding initially occurred in the loaded end for a load of 37.4 kN and subsequently propagated from the loaded end toward the free end. While approaching failure, the entire interface had undergone a substantial amount of slip.

The typical displacement and strain evolution with a load increment is shown in Fig. 11. The load stages from A to F are the key stages listed on the load-slip curve, as shown in Fig. 9. The displacement distributions intuitively reflect that the CFRP displacement increased on the interface and gradually expanded from the loaded end toward the free end, whereas the steel displacements were very small. The steel strain also indicates that only the rigid body displacement occurred during loading. The gradual debonding process of the interface is directly revealed in Fig. 11.

On the CFRP surface of the strain gauge group, fourteen strain gauges were placed at intervals of 25 mm in the longitudinal direction, as shown in Fig. 12. The typical axial strain distribution obtained by the stereo-DIC together with the strain gauge results are presented in Fig. 13(a). It's worth mentioning that one strain gauge became invalid in the experiment so that there are only thirteen strain gauge data in the strain curve. The continuous DIC result corresponded with the discrete strain gauge data. The average relative error between DIC and strain gauge data was 3.04% with a maximum relative error of 4.65%. The local fluctuations of DIC strain can be attributed to the non-uniform distribution of the adhesive and the non-homogenous characteristics of the composite material. As mentioned, the relative slip was previously derived from the integral operation of strain data measured by strain gauges (Yu *et al.* 2012). To obtain the slip with the integral method, the strain data of the invalid strain gauge was added through

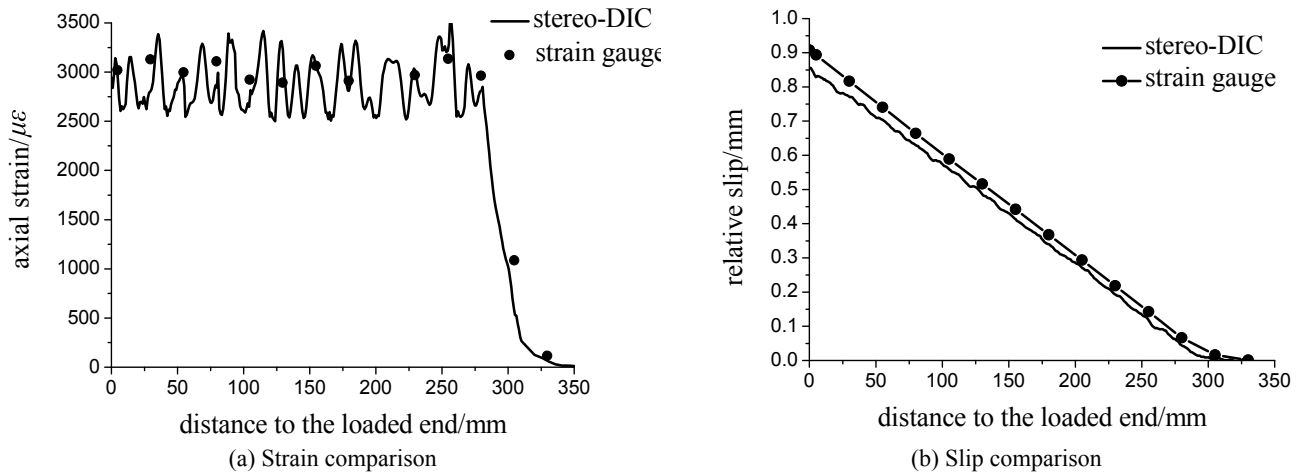


Fig. 13 Comparisons between DIC and strain gauge under 33.4 kN

theoretical calculation. Fig. 13(b) shows the comparison of the slips obtained using the DIC method and the integral method based on strain gauges. The results demonstrate that the slips calculated using the integral method were slightly larger than the DIC results. This is mainly because the integral method cannot account for the effect of the steel displacement.

In contrast with the limited strain gauges that provide strain data at discrete points, the DIC can obtain a sufficient amount of continuous strain data. Thus, the interfacial shear stress can be derived via differential operation of the continuous strain distribution. By combining the obtained continuous shear stress distribution with the slip distribution in Fig. 10, the bond-slip relationship of the CFRP-to-steel interface was easily obtained. Consider the load of 33.4 kN as an example. It can be observed from Fig. 14 that the shear stress increased and then decreased with an increase in relative slip. Before the shear stress attained its peak value, it increased as relative slip increased. Thereafter, the shear stress gradually decreased and approached zero with a significant increase in relative slip. It should be noted that the bond-slip relationship in this study was the preliminary result based on the measured relative slip and the differential operation of the measured strain, more precise bond-slip relationship can be obtained via fitting procedure (Wang *et al.* 2016).

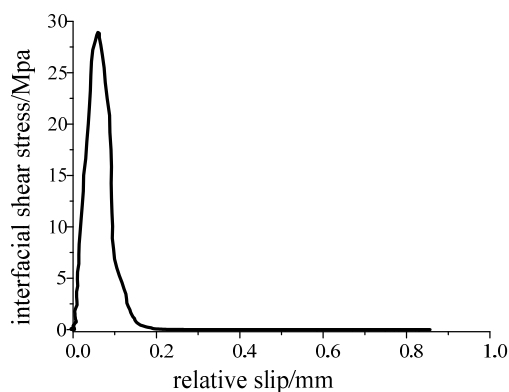


Fig. 14 Bond-slip relationship under 33.4 kN

4.2 Buckling behavior investigation of CFRP-strengthened SHS steel column

Instead of installing displacement transducers and strain gauges on the anticipated buckling area, the DIC technique can capture the full-field buckling shape and obtain the deformation of the exact buckling area. The failure mode can also be recorded. The out-of-plane displacement fields reflecting the buckling shape, which were obtained via the multi-camera DIC system, are shown in Fig. 15.

The typical failure mode for a short SHS steel column is yielding and subsequent symmetric local buckling. The buckling shape of the example column is presented in Fig. 16. Inward and outward buckling were observed on all four sides at the column ends. As with the buckling mode of the short SHS column that was previously described in the literature (Shaah and Fam 2006), two opposite sides—side A and side C—buckled outward and the remaining two sides—side B and side D—buckled inward.

The load-displacement curves for the short SHS steel columns wrapped and unwrapped with CFRP sheets are shown in Fig. 17. The ultimate load capacity of the CFRP-strengthened SHS steel column was significantly higher than that of the control column. Quantitative comparisons of the ultimate load capacity, axial displacement and elastic stiffness between the columns are tabulated in Table 2. The

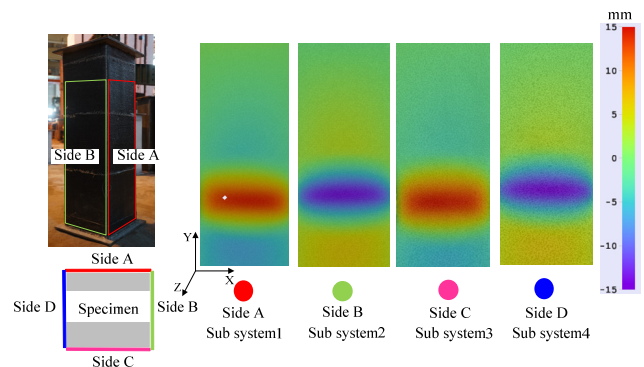


Fig. 15 Out-of-plane displacement fields in four stereo-DIC subsystems

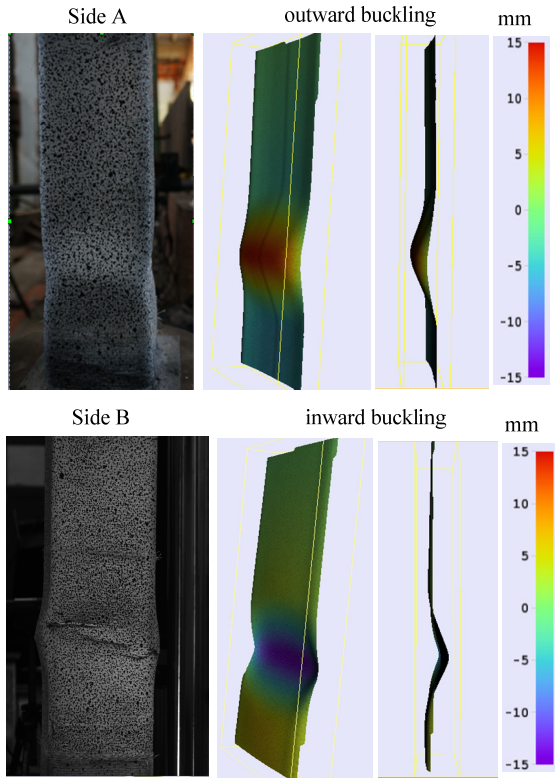


Fig. 16 Buckling mode of short SHS steel column

increment of these aspects for the CFRP-strengthened SHS steel column relative to the control column are also given. A strength enhancement of 17% and a stiffness gain of 52% were achieved for the SHS steel column with two layers of CFRP in the transverse and longitudinal directions.

For the curve of the CFRP-strengthened column, three abrupt reductions in load were observed in the descending stage, which indicates the CFRP delamination. The

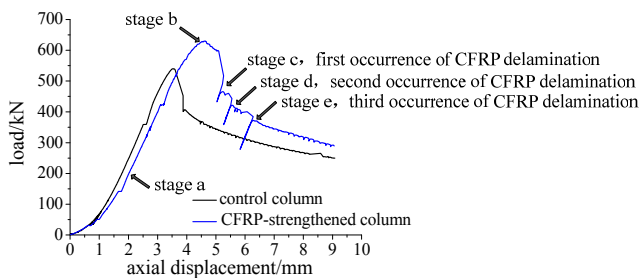


Fig. 17 Load-displacement curves

Table 2 Comparisons of the ultimate load capacity and the stiffness

Aspect	Control column	CFRP-strengthened column	Increment
Maximum load (kN)	539.98	630.15	17%
Axial displacement (mm)	3.53	4.61	31%
Elastic stiffness (kN/mm)	22.58	34.32	52%

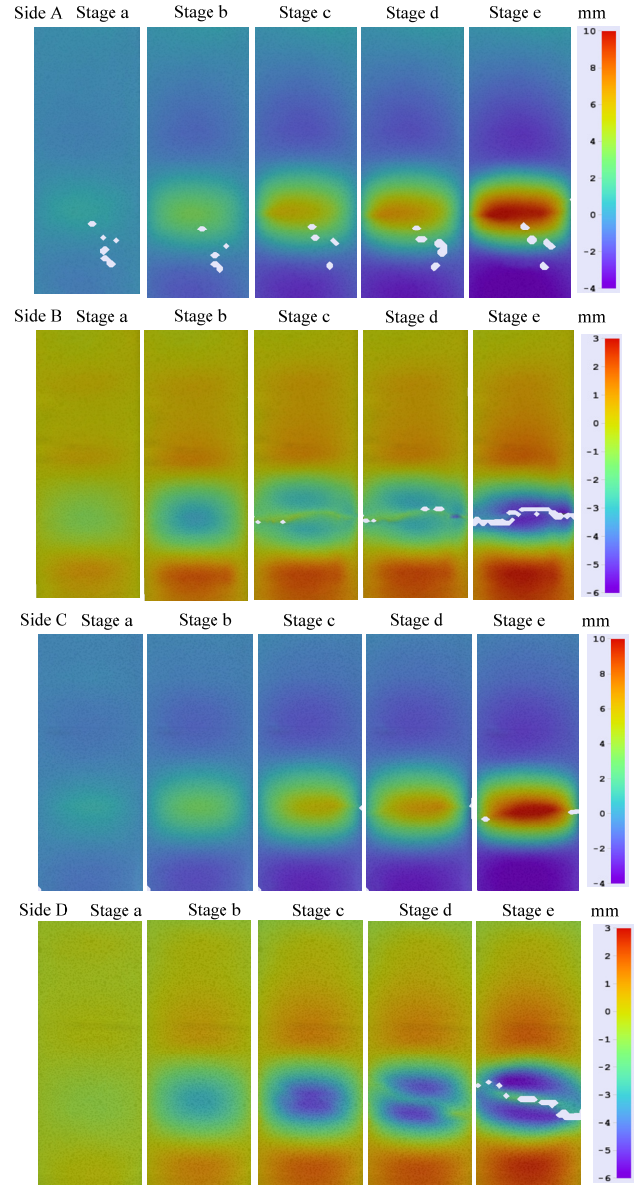


Fig. 18 Out-of-plane displacement evolution of the CFRP-strengthened SHS steel column

delamination is also directly reflected on the displacement contours of the four key stages depicted in Fig. 17, as shown in Fig. 18. The abrupt reduction in load can be attributed to the sudden absence of constraint from the CFRP. It is clearly seen from Fig. 18 that the CFRP delamination was only observed on the two opposite sides of the inward local buckling. Combining Fig. 17 and Fig. 18, the typical deformation process can be concluded as follows: in the rising stage a, out-of-plane displacement occurred on the column ends. Toward stage b of the maximum load, outward displacement on side A/C and inward displacement on side B/D significantly increased to form notable deformed nuclei. Upon reaching stage c, a band traversed the deformed nucleus on side B/D, which indicates the occurrence of CFRP delamination on the inward buckling side. Stage d was the second occurrence of CFRP delamination with a continuous increase in out-of-plane displacement. Stage e referred to the third occurrence

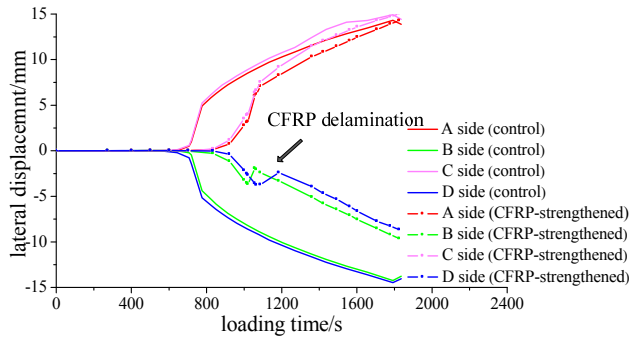


Fig. 19 Out-of-plane displacement with the loading time

of CFRP delamination; the band in the deformed nucleus split, presenting the actual performance of CFRP rupture. Meanwhile, on the outward buckling side A/C, rupture of the fibers was observed near the corners. No debonding of CFRP was observed prior to the ultimate load, which confirms that the bond between the CFRP and the steel was perfect.

Fig. 19 shows the out-of-plane displacement versus loading time on the four sides of the two columns, as measured by the multi-camera DIC system. The out-of-plane deformation was significantly restrained by the CFRP sheets in the CFRP-strengthened column compared with the control column. The fluctuation region on the curve of the CFRP-strengthened column is attributed to the occurrence of CFRP delamination on the inward buckling side B/D. The effective restraint of the CFRP sheets delayed the onset of out-of-plane deformation and local buckling, reduced the maximum out-of-plane displacement and enhanced the deformability. The figure also indicates that the restraint of the CFRP sheets to the inward buckling side B/D was superior to the outward buckling side A/C.

5. Conclusions

The effectiveness of the DIC technique in studying the bond and buckling behaviors of CFRP-steel composite members was demonstrated in this paper. Compared with the conventional electrometric techniques, the DIC technique can provide full-field deformation distribution. The entire failure process can be intuitively recorded.

- The bond behavior between the CFRP plate and the steel was tested using the stereo-DIC technique. Continuous CFRP and steel displacements can be obtained; thus, the continuous relative slip can be directly measured using this method. The bond-slip relationship of the CFRP plate-to-steel interface can be easily obtained from the DIC data.
- The first insight into the buckling behavior of a CFRP-strengthened SHS steel column using a multi-camera DIC system was presented. The multi-camera DIC system consists of four stereo-DIC subsystems that can capture the exact process of deformation and buckling. The experimental study shows that the application of CFRP sheets delayed the occurrence of local buckling and increased the

ultimate load capacity and elastic stiffness of the SHS steel column.

This study indicates that the stereo-DIC technique can provide effective measurements in the behavior investigation of CFRP-steel composite members.

Acknowledgments

The authors acknowledge the financial support from the National Natural Science Foundation of China [under Grant nos: 11332012, 11327201 and 11532005]; the National Key Technology R&D Program [under Grant no: 2014BAK11B04]; the Fundamental Research Funds for the Central Universities and the Jiangsu Innovation Program for Graduate Education [under Grant no: KYLX15_0094].

References

- Abdelrahman, K. and El-Hacha, R. (2011), "Behavior of large-scale concrete columns wrapped with CFRP and SFRP sheets", *J. Compos. Constr.*, **16**(4), 430-439.
- Ali-Ahmad, M., Subramaniam, K. and Ghosn, M. (2006), "Experimental investigation and fracture analysis of debonding between concrete and FRP sheets", *J. Eng. Mech.*, **132**(9), 914-923.
- Bakis, C.E., Bank, L.C., Brown, V.L., Cosenza, E., Davalos, J.F., Lesko, J.J. and Triantafillou, T.C. (2002), "Fiber-reinforced polymer composites for construction—state-of-the-art review", *J. Compos. Constr.*, **6**(2), 73-87.
- Bocciarelli, M., Colombi, P., Fava, G. and Poggi, C. (2009), "Prediction of debonding strength of tensile steel/CFRP joints using fracture mechanics and stress based criteria", *Eng. Frac. Mech.*, **76**(2), 299-313.
- Busca, D., Fazzini, M., Lorrain, B., Mistou, S., Karama, M. and Pastor, M.L. (2014), "High-speed stereo digital image correlation: application to biaxial fatigue", *Strain*, **50**(5), 417-427.
- Daud, R.A., Cunningham, L.S. and Wang, Y.C. (2015), "Static and fatigue behaviour of the bond interface between concrete and externally bonded CFRP in single shear", *Eng. Struct.*, **97**, 54-67.
- Fagerholt, E., Børvik, T. and Hopperstad, O.S. (2013), "Measuring discontinuous displacement fields in cracked specimens using digital image correlation with mesh adaptation and crack-path optimization", *Opt. Lasers Eng.*, **51**(3), 299-310.
- Fawzia, S., Zhao, X.L. and Al-Mahaidi, R. (2010), "Bond-slip models for double strap joints strengthened by CFRP", *Comp. Struct.*, **92**(9), 2137-2145.
- Ghiassi, B., Xavier, J., Oliveira, D.V. and Lourenco, P.B. (2013), "Application of digital image correlation in investigating the bond between FRP and masonry", *Compos. Struct.*, **106**, 340-349.
- Hadji, L., Daouadi, T.H., Meziane, M.A.A. and Bedia, E.A.A. (2016), "Analyze of the interfacial stress in reinforced concrete beams strengthened with externally bonded CFRP plate", *Steel Compos. Struct., Int. J.*, **20**(2), 413-429.
- Ke, X.D., Schreier, H.W., Sutton, M.A. and Wang, Y.Q. (2011), "Error assessment in stereo-based deformation measurements", *Exp. Mech.*, **51**(4), 423-441.
- Kumar, R.L.V., Bhat, M.R. and Murthy, C.R.L. (2013), "Experimental analysis of composite single-lap joints using digital image correlation and comparison with theoretical models", *J. Reinf. Plast. Comp.*, **32**(23), 1858-1876.

- Liu, C., Chen, Z.N., Ding, L.N., Wu, G. and He, X.Y. (2013), "360-degree-full-surface digital image correlation system in civil engineering applications", *Proceedings of Jointed Conference on International Conference on Experimental Mechanics 2013 and the 12th Asian Conference on Experimental Mechanics*, Bangkok, Thailand, November.
- Malesa, M., Malowany, K., Tomczak, U., Siwek, B., Kujawińska, M. and Siemińska-Lewandowska, A. (2013), "Application of 3D digital image correlation in maintenance and process control in industry", *Comput. Ind.*, **64**(9), 1301-1315.
- Pan, B., Wu, D.F. and Yu, L.P. (2012), "Optimization of a three-dimensional digital image correlation system for deformation measurements in extreme environments", *Appl. Opt.*, **51**(19), 4409-4419.
- Pan, B., Li, K. and Tong, W. (2013), "Fast, robust and accurate digital image correlation calculation without redundant computations", *Exp. Mech.*, **53**(7), 1277-1289.
- Park, J.W. and Yoo, J.H. (2015), "Flexural and compression behavior for steel structures strengthened with Carbon Fiber Reinforced Polymers sheet", *Steel Compos. Struct., Int. J.*, **19**(2), 441-465.
- Peters, W.H. and Ranson, W.F. (1982), "Digital imaging techniques in experimental stress analysis", *Opt. Eng.*, **21**(3), 213427-213427.
- PMLAB (2014), Digital Image Correlation Software PMLAB DIC-3D_2014a; Nanjing PMLAB*Sensor Tech. Co., Ltd., Nanjing, China. <http://www.pmlab.com.cn>
- Shaat, A. and Fam, A.Z. (2006), "Axial loading tests on short and long hollow structural steel columns retrofitted using carbon fibre reinforced polymers", *Can. J. Civil Eng.*, **33**(4), 458-470.
- Shaat, A. and Fam, A.Z. (2009), "Slender steel columns strengthened using high-modulus CFRP plates for buckling control", *J. Compos. Constr.*, **13**(1), 2-12.
- Shao, X.X., Dai, X.J. and He, X.Y. (2015), "Noise robustness and parallel computation of the inverse compositional Gauss-Newton algorithm in digital image correlation", *Opt. Lasers Eng.*, **71**, 9-19.
- Shi, J.W., Zhu, H., Wu, Z.S., Seracino, R. and Wu, G. (2012), "Bond behavior between basalt fiber-reinforced polymer sheet and concrete substrate under the coupled effects of freeze-thaw cycling and sustained load", *J. Compos. Constr.*, **17**(4), 530-542.
- Sutton, M.A., Orteu, J.J. and Schreier, H. (2009), *Image Correlation for Shape, Motion and Deformation Measurements: Basic Concepts, Theory and Applications*, Springer Science & Business Media, LLC, New York, NY, USA.
- Teng, J.G., Yu, T. and Fernando, D. (2012), "Strengthening of steel structures with fiber-reinforced polymer composites", *J. Constr. Steel Res.*, **78**, 131-143.
- Wang, Y.Q., Sutton, M.A., Ke, X.D., Schreier, H.W., Reu, P.L. and Miller, T.J. (2011), "On error assessment in stereo-based deformation measurements", *Exp. Mech.*, **51**(4), 405-422.
- Wang, H.T., Wu, G., Dai, Y.T. and He, X.Y. (2016), "Determination of the bond-slip behavior of CFRP-to-steel bonded interfaces using digital image correlation", *J. Reinf. Plast. Comp.*, **35**(18), 1353-1367.
- Wu, C., Zhao, X.L., Duan, W.H. and Al-Mahaidi, R. (2012), "Bond characteristics between ultra high modulus CFRP laminates and steel", *Thin-Wall. Struct.*, **51**, 147-157.
- Xavier, J., De Jesus, A.M.P., Morais, J.J.L. and Pinto, J.M.T. (2012), "Stereovision measurements on evaluating the modulus of elasticity of wood by compression tests parallel to the grain", *Constr. Build. Mater.*, **26**(1), 207-215.
- Yu, T., Fernando, D., Teng, J.G. and Zhao, X.L. (2012), "Experimental study on CFRP-to-steel bonded interfaces", *Compos. Part B*, **43**(5), 2279-2289.
- Zhao, X.L. and Zhang, L. (2007), "State-of-the-art review on FRP strengthened steel structures", *Eng. Struct.*, **29**(8), 1808-1823.
- Zhu, H., Wu, G., Shi, J.W., Liu, C. and He, X.Y. (2014), "Digital image correlation measurement of the bond-slip relationship between fiber-reinforced polymer sheets and concrete substrate", *J. Reinf. Plast. Comp.*, **33**(17), 1590-1603.

CC